

Multi-orbital Effects in Optical Properties of Vanadium Sesquioxide

Jan M. Tomczak

Research Institute for Computational Sciences, AIST, Tsukuba, 305-8568 Japan
Japan Science and Technology Agency, CREST

Silke Biermann

Centre de Physique Théorique, Ecole Polytechnique, 91128 Palaiseau Cedex, France
Japan Science and Technology Agency, CREST

E-mail: jan.tomczak@polytechnique.edu

Abstract. Vanadium sesquioxide, V_2O_3 , boasts a rich phase diagram whose description necessitates the accounting for many-body Coulomb correlations. Spectral properties of this compound have been successfully addressed within dynamical mean field theory to an extent that results of recent angle resolved photoemission experiments have been correctly predicted. While photoemission spectroscopy probes the occupied part of the one-particle spectrum, optical experiments measure transitions into empty states and thus provide complementary information. In this work, we focus on the optical properties of V_2O_3 in its paramagnetic phases by employing our recently developed “generalized Peierls approach”. Compared to experiments, we obtain results in overall satisfactory agreement. Further, we rationalize that the experimentally observed temperature dependence stems from the different coherence scales of the involved charge carriers.

1. Introduction

Vanadium sesquioxide, V_2O_3 , has been the subject of extensive theoretical and experimental studies for now more than three decades. It is considered as *the* prototype compound, that undergoes a Mott-Hubbard transition [1, 2] in its purest form. Indeed, the high-temperature ($T > T_{\text{Néel}}$) metal-insulator transition upon chemical substitution, $(V_{1-x}Cr_x)_2O_3$, is isostructural and no magnetic order is acquired. Early theoretical approaches resorted to the Hubbard model to explain the electronic properties of V_2O_3 . However, over the years, experiments indicated that the physics of this material is more involved and a realistic multi-orbital setup is needed for the complexity of the correlation effects taking place. For reviews see e.g. [1, 2, 3].

The field of correlated materials gained major momentum from the development of dynamical mean field theory (DMFT) [4]. In combination with standard density functional based methods like the local density approximation (LDA) the calculation

of spectral properties of materials with strong electronic Coulomb interactions became possible. Over the past years, LDA+DMFT enlightened our understanding of materials such as transition metals, their oxides or sulphides, as well as f-electron compounds [5]. Several works highlighted the applicability of the technique to V_2O_3 [6, 7, 8, 9, 10, 11]. In our previous work [11], we find that the metal-insulator transition is not due to the Brinkman-Rice mechanism [12] in its single-band form, but results from the impact of Coulomb correlations on the crystal-field splitting. Owing to its octahedral oxygen surrounding, the vanadium 3d-orbitals split into two e_g^σ and three lower lying $2g$ orbitals. The two manifolds of bands are isolated in energy both from each other and from other orbitals. The trigonal part of the crystal field further splits the $2g$ into an a_{1g} and two lower lying degenerate e_g^π orbitals. The local Coulomb correlations result in an increased a_{1g} - e_g^π -splitting with respect to the LDA, causing a charge transfer that pushes a_{1g} spectral weight above the Fermi level. By computing momentum-resolved spectral functions [13, 14, 11], we made explicit predictions for angle-resolved photoemission experiments. Recent measurements on $(V_{1-x}Cr_x)_2O_3$ ($x=0.011$) [15] nicely agree with the theoretical spectra, further validating our current understanding of this compound.

2. Optical properties – prelude

An experimental probe complementary to photoemission is optical spectroscopy, which is commonly analyzed in terms of the optical conductivity [16]

$$\Re\sigma^{\alpha\beta}(\omega) = \frac{2\pi e^2 \hbar}{V} \sum_{\mathbf{k}} \int d\omega' \frac{f(\omega') - f(\omega' + \omega)}{\omega} \text{tr} \left\{ A_{\mathbf{k}}(\omega' + \omega) v_{\mathbf{k},\alpha} A_{\mathbf{k}}(\omega') v_{\mathbf{k},\beta} \right\} \quad (1)$$

that is given by a convolution of spectral functions $A_{\mathbf{k}}(\omega)$ [‡]. The transitions are weighted by dipole matrix elements, called Fermi velocities, $v_{\mathbf{k},\alpha}$, and the Fermi functions $f(\omega)$ select the range of occupied and empty states, respectively. V is the unit-cell volume, α, β denote cartesian coordinates, and $\Re\sigma^{\alpha\beta}$ is the response in α -direction for a light polarization along β . Both spectral functions and velocities are matrices in the basis of localized orbitals, which we index by $L = (n, l, m, \gamma)$, with the usual quantum numbers (n, l, m) , while γ labels the individual atoms in the unit cell. While the computation of the Fermi velocities is straight-forward e.g. in a plane-wave basis, their evaluation becomes tedious when using localized orbitals as required by many-body approaches such as LDA+DMFT. To this end, we employ the recently generalized Peierls approach [3, 18, 19], which we briefly summarize in Appendix A.1.

In their pioneering work, Rozenberg *et al* [20] analyzed the optical conductivity of V_2O_3 from the model perspective. It was concluded that the phenomenology of the temperature dependence in the conductivity can be understood by appealing to the physics of the one-band Hubbard model. In the current work, we will substantiate and extend these observations, based on a realistic multi-band setup.

[‡] In the case of a single orbital, vertex-corrections vanish in the limit of infinite lattice coordination [17]. Therewith, the response can be expressed in terms of spectral functions. In the general multi-orbital case this is an approximation.

3. Optical properties – results

Our calculation of the optical conductivity is based on the previous LDA+DMFT electronic structure computation of Ref. [11], which used a one-particle Hamiltonian that was downfolded [21, 22] to the vanadium $\hat{2}g$ orbitals. Since optical experiments normally probe a much wider frequency range, we employ an unfolding scheme that includes higher energy states on the LDA level. Details are summarized in Appendix A.2.

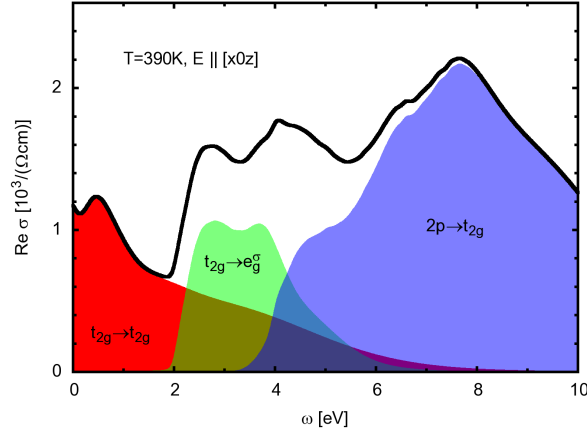


Figure 1. Theoretical optical conductivity of V_2O_3 at $T \approx 390$ K for a light polarization $E \parallel [x\ 0\ z]=[0.13, 0.0, 0.041]$. Contributions from different energy sectors (see Appendix A.2) : $\hat{2}g \rightarrow \hat{2}g$ (red), $\hat{2}g \rightarrow e_g^\sigma$ (green), $\text{O}2p \rightarrow \hat{2}g$ (blue).

Figure 1 shows our theoretical optical conductivity for V_2O_3 at $T=390$ K for the indicated light polarization. While in the Kohn-Sham spectrum, the $\hat{2}g$ and e_g^σ bands are well separated, the correlations – accounted for by LDA+DMFT for the $\hat{2}g$ orbitals only [11] – result in an intra- $\hat{2}g$ conductivity that has weight up to energies well beyond the onset of transitions into the e_g^σ at about 2 eV. Contributions stemming from transitions from the occupied oxygen 2p orbitals into the $\hat{2}g$ occur from around 3.5 eV onwards.

Before turning to a more detailed analysis of the different orbital contributions we compare our results to experimental data (see figure 2). First, we notice the discrepancies *between the experiments* : Recent measurements on single crystals [24] agree well with previous single crystal experiments [20], but they are at variance with measurements using a polycrystalline film [23]. While the use of polycrystalline samples especially in a metal might be an issue, so is the fact that both single crystal experiments were performed up to energies of only a few eVs although the extraction of the conductivity involves a Kramers-Kronig transform. The low energy shape of the theoretical conductivity resembles the polycrystalline conductivity, but the absolute values differ. As to the single crystal one, we note that the order of magnitude compares favourably, while the shape tends to be comparable with the high temperature curves only.

At high energies, we see that both the onset and the shape of oxygen 2p derived contributions agree with experiment. The unfolding scheme that uses the 2p bands from LDA is thus a good approximation. This seems not to be true for transitions into e_g^σ orbitals : Compared with experiment [23], we realize that spectral weight is too sharply defined and no identification of particular structures is possible. This calls for an LDA+DMFT calculation that includes all vanadium 3d orbitals.

We now turn to a detailed analysis of orbital effects in the optical conductivity. This is a topic that has not at all been dealt with so far, since previous work neglected inter-band transitions altogether [24].

At low energy only a small Drude-like tail appears. This can be understood from the underlying electronic structure. Indeed, the metallic character of V_2O_3 is mainly a result from a_{1g} charge carriers that have spectral weight at the Fermi level only in a very limited region of the Brillouin zone (BZ), as can be seen in figure 4 of Ref. [11].

As can also be inferred from that work, the local spectral functions of a_{1g} and e_g^π character display a pseudo-gap-like behaviour, and peak at finite energies rather than at the Fermi level, accounting for the feature seen at 0.5 eV in the conductivity. The latter originates from two types of transitions§ : At energies lower than 0.6 eV the spectral weight is mainly due to transitions from the a_{1g} into low lying e_g^π orbitals, that are restricted to a small region in the BZ, whereas at slightly higher energies, 0.6 eV and above, contributions are in majority deriving from e_g^π to e_g^π transitions, which are possible in a wide region of the BZ, yet are less prominent at the Γ -point.

At this point we again use our knowledge about the electronic structure of the compound: Reference [11] established an important orbital dependence of the quasi-particle coherence scale. Indeed, down to 390 K, e_g^π excitations are far from being coherent : The imaginary part of the e_g^π self-energy reaches -0.45 eV at the Fermi level, while a_{1g} excitations have reached their coherence regime in our calculation [11, 3]. Therewith (e_g^π) a_{1g} carriers are (not) particularly sensitive to changes in temperature. As discussed above, the low-energy (< 0.6 eV) optical response is determined by a_{1g} - e_g^π transitions, while above 0.6 eV e_g^π - e_g^π transitions become dominant. Given these two facts, one can – even without explicit calculations – make some predictions about the behaviour of the optical response when the temperature is raised: Upon heating, the purely e_g^π -derived contributions will not change as much as will those that involve the a_{1g} orbitals, so that the low-energy response will be more sensitive than the weight beyond 0.6 eV. In particular, a broadening (and thus reduction in height) is expected for the very low energy part. This gives a natural explanation for the dip behaviour that is observed in the experiments when the temperature is raised above ~ 450 K (see figure 1 in Ref. [24] or our figure 2) ||. Explicit calculations as a function of temperature

§ The following is inferred from “momentum resolved optics”, i.e. from distinguishing contributions of different points in the Brioullin zone (not shown, see [3]).

|| Ref. [24] has invoked the change of the lattice constants upon heating in order to explain this dip. It is clear that the mechanism based on the orbital-selective coherence that emerges from our work could not have been observed in the calculation of Baldassarre *et al*, since, there, inter-band transitions were

(including inter-band transitions) would be desirable to confirm the picture emerging from our results. This challenging project is left for future work.

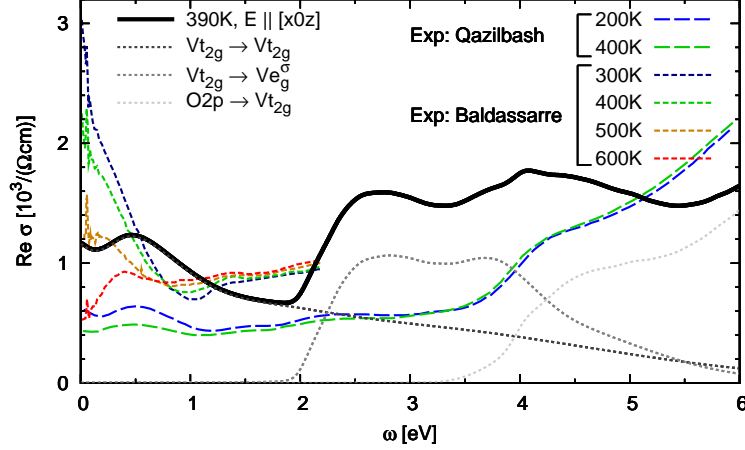


Figure 2. Theoretical and experimental conductivity of V_2O_3 . Theory (same polarization as in figure 1) : total (bold black), orbital contributions (shades of gray, dotted). Experiments : polycrystalline film, ($T=200, 400$ K) Qazilbash *et al* [23] (blue, green, long dashed), single crystal ($T=300\text{--}600$ K) Baldassarre *et al* [24] (blue to red, short dashed).

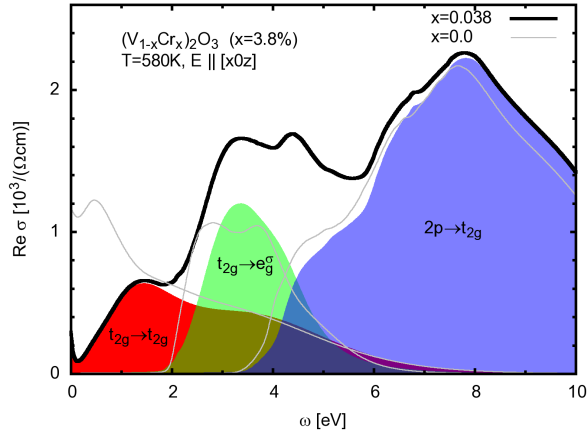


Figure 3. Theoretical optical conductivity of $(V_{1-x}Cr_x)_2O_3$, $x=3.8\%$ at $T = 580$ K for a light polarization $E \parallel [x0z]=[0.13, 0.0, 0.0415]$. Contributions from different energy sectors : $\hat{2}g \rightarrow \hat{2}g$ (red), $\hat{2}g \rightarrow e_g^\sigma$ (green), $O2p \rightarrow \hat{2}g$ (blue). Gray lines show the results of pure V_2O_3 (figure 1) for comparison.

In figure 3 we show theoretical results for the insulator $(V_{1-x}Cr_x)_2O_3$ ($x=3.8\%$). As discussed previously [11], we have low but finite spectral weight at the Fermi level, which results in some optical weight at low frequency. Unfortunately, no experimental data is available for this composition. Compared with pure V_2O_3 , we note the suppression neglected (see their footnote 26 and our discussion in Appendix A.1).

of low energy spectral weight and the clear distinction of transitions into the $2g$ upper Hubbard bands at ~ 4 eV.

4. Conclusions

In conclusion, we presented calculations of the optical conductivity of V_2O_3 in its paramagnetic phases using the generalized Peierls approach. We obtain good agreement with experiment and propose an explanation for the experimentally witnessed temperature dependence of the response as a signature of the orbital selective coherence of the system. Our unfolding scheme to include higher energy orbitals captures well the transitions involving oxygen states, but reveal the necessity to include all 3d orbitals in an LDA+DMFT electronic structure calculation for this compound.

Acknowledgments

We thank M. M. Qazilbash, M. Marsi and A. I. Lichtenstein for discussions on optical and photoemission spectroscopy. Moreover, we thank our coauthors of Ref. [11], and in particular A. I. Poteryaev, for the collaboration on the electronic structure of V_2O_3 that was our starting point. JMT kindly acknowledges support by the Ecole Polytechnique, where this work began. This work was supported by the French ANR under project CORRELMAT, and by Idris, Orsay, under project No. 081393.

Appendix A. Details of the formalism

Appendix A.1. Generalized Peierls substitution approach to Fermi velocities

The Fermi velocities in (1) are given by elements of the momentum operator \mathcal{P} :

$$v_{\mathbf{k},\alpha}^{L'L} = \frac{1}{m} \langle \mathbf{k}L' | \mathcal{P}_\alpha | \mathbf{k}L \rangle \quad (\text{A.1})$$

$L=(n,l,m,\gamma)$ and γ labels atoms in the unit-cell. In plane waves (A.1) is easily calculated, while using a localized Wannier-like basis $\chi_{\mathbf{R}L}(\mathbf{r}) = \langle \mathbf{r} | \mathbf{R}L \rangle = \sum_{\mathbf{k}} e^{-i\mathbf{k}\mathbf{R}} \langle \mathbf{r} | \mathbf{k}L \rangle$ renders the evaluation tedious. Inspired by the Peierls substitution approach [16] of lattice models, we can separate the above into [3, 18, 19] :

$$v_{\mathbf{k},\alpha}^{L'L} = \frac{1}{\hbar} \left(\partial_{k_\alpha} \mathbf{H}_{\mathbf{k}}^{L'L} - i(\rho_{L'}^\alpha - \rho_L^\alpha) \mathbf{H}_{\mathbf{k}}^{L'L} \right) + \mathcal{F}_{\mathbf{H}} [\{\chi_{\mathbf{R}L}\}] \quad (\text{A.2})$$

The terms in brackets are the Fermi velocity in the Peierls approximation, which is here generalized to multi-atomic unit-cell : ρ_L^α is the α -component of the position of atom γ within the unit-cell. This velocity is easy to evaluate since it involves only elements of the Hamiltonian. Crucial is that $\mathcal{F}_{\mathbf{H}}[\{\chi_{\mathbf{R}L}\}]$ reduces to intra-atomic contributions in the limit of strongly localized orbitals $\chi_{\mathbf{R}L}$ [3], which makes the generalized Peierls velocity a good approximation for e.g. 3d and 4f systems.

Finally, we ask if the computation of the Fermi velocities is really necessary in practice, or if one could also resort to a simpler approximation consisting in

simply omitting the Fermi velocities. Due to its simplicity, this approximation is in fact relatively popular to obtain qualitative trends of optical properties in correlated systems [25, 24]. Since then the conductivity is then a simple convolution of spectral functions, inter-band transitions ($L \neq L'$) are neglected and intra-band transitions not properly weighted. As an illustration, we show in figure A1 a comparison of the optical conductivity calculated within the generalized Peierls formalism compared to the one computed from the simple convolution of spectral functions¶: Besides the obvious discrepancy in absolute value, omitting the Fermi velocities results in a noticeable change in shape, too. This is owing to the momentum dependence of the matrix elements that favours certain regions in the Brillouin zone, while attenuating others.

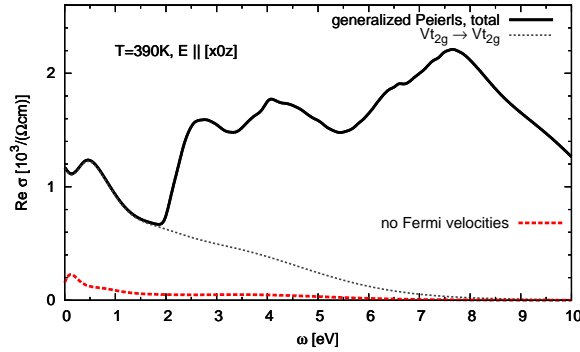


Figure A1. Generalized Peierls conductivity versus “no velocity approximation”.

Appendix A.2. Upfolding scheme for higher energy transitions

Although the treatment of many-body correlations can often be cast into an effective low energy, downfolded system, the range of its validity is usually far exceeded by optical measurements. Thus it is desirable to allow for optical transitions into higher energy orbitals. Also, the computation of the Fermi velocities and the downfolding procedure do not commute [16], and hence it makes a difference to which Hamiltonian the generalized Peierls approach is applied. As a matter of fact, the Wannier functions of a full Hamiltonian are more localized than for the downfolded one, whereby the Peierls approximation becomes more accurate⁺. The key quantity for the conductivity is the orbital trace in (1). For any unitary transformation $U_{\mathbf{k}}$ holds

$$\text{tr}\{v_{\mathbf{k}} A_{\mathbf{k}}(\omega') v_{\mathbf{k}} A_{\mathbf{k}}(\omega' + \omega)\} = \text{tr}\{U_{\mathbf{k}}^\dagger v_{\mathbf{k}} U_{\mathbf{k}} \tilde{A}_{\mathbf{k}}(\omega') U_{\mathbf{k}}^\dagger v_{\mathbf{k}} U_{\mathbf{k}} \tilde{A}_{\mathbf{k}}(\omega' + \omega)\} \quad (\text{A.3})$$

where we defined $\tilde{A}_{\mathbf{k}} = U_{\mathbf{k}}^\dagger A_{\mathbf{k}} U_{\mathbf{k}}$. In the case of a pure band-structure calculation (no self-energy), we can choose the transformation such that it performs the downfolding, i.e. the spectral functions $\tilde{A}_{\mathbf{k}}$ acquire a block-diagonal form. We shall distinguish between

¶ In order to have comparable scales, we chose for the latter case $v_{\mathbf{k}} = r_0 \mathbb{1}$, with the Bohr-radius r_0 .

⁺ Indeed the downfolding can be viewed as a unitary transformation that block-diagonalizes the Hamiltonian (see below). The change in accuracy manifests itself in the basis dependence of the optical conductivity within the Peierls approach.

the low energy (\mathcal{L}) and the high energy block (\mathcal{H}) : An LDA+DMFT calculation will add local Coulomb interactions only to the former *after* the block-diagonalization, which results in a self-energy that lives in this sub-block, while high energy bands remain unchanged and the block-diagonality is retained. Clearly the downfolding procedure is not exact in the many-body framework. Indeed the matrices that block-diagonalize the true interacting system also depend on frequency due to the dynamical nature of the self-energy. Yet, when granting the approximative validity of the downfolding, and using the $U_{\mathbf{k}}$ of the band-structure calculation, we can specify

$$\tilde{v}_{\mathbf{k}} = \begin{pmatrix} V_1 & W \\ W^\dagger & V_2 \end{pmatrix}, \tilde{A}_{\mathbf{k}}(\omega') = \begin{pmatrix} L & 0 \\ 0 & H \end{pmatrix}, \tilde{A}_{\mathbf{k}}(\omega' + \omega) = \begin{pmatrix} \bar{L} & 0 \\ 0 & \bar{H} \end{pmatrix} \quad (\text{A.4})$$

with $\tilde{v}_{\mathbf{k}} = U_{\mathbf{k}}^\dagger v_{\mathbf{k}} U_{\mathbf{k}}$. The many-body spectra L, \bar{L} are substituted into the \mathcal{L} -sector, while H, \bar{H} of the \mathcal{H} -sector stem from the initial band-structure, and (A.3) reads

$$LV_1\bar{L}V_1 + LW\bar{H}W^\dagger + HV_2\bar{H}V_2 + HW^\dagger\bar{L}W \quad (\text{A.5})$$

For transitions within the \mathcal{L} -block, the velocity V_1 appears, which is the \mathcal{L} -block of the *transformed* velocity. It is different from the element computed *after* the downfolding. With the above, we moreover include transitions from, to and within the high energy block*. Comparing to experiments then allows to assess whether correlation effects substantially modify also the spectrum of downfolded orbitals, or whether for them the initial band-structure is satisfying (see above for the V_2O_3 case).

References

- [1] N. F. Mott. *Metal-Insulator transition*. Taylor and Francis, London, 1990.
- [2] M. Imada, A. Fujimori, and Y. Tokura. Metal-insulator transitions. *Rev. Mod. Phys.*, 70(4):1039–1263, Oct 1998.
- [3] Jan M. Tomczak. *Spectral and Optical Properties of Correlated Materials*. PhD thesis, Ecole Polytechnique, France, 2007.
- [4] A. Georges, G. Kotliar, W. Krauth, and M. J. Rozenberg. Dynamical mean-field theory of strongly correlated fermion systems and the limit of infinite dimensions. *Rev. Mod. Phys.*, 68(1):13, Jan 1996.
- [5] G. Kotliar and D. Vollhardt. Strongly correlated materials: Insights from dynamical mean-field theory. *Physics Today*, 57(3):53, 2004.
- [6] K. Held, G. Keller, V. Eyert, D. Vollhardt, and V. I. Anisimov. Mott-Hubbard metal-insulator transition in paramagnetic V_2O_3 : An LDA+DMFT (QMC) study. *Phys. Rev. Lett.*, 86(23):5345–5348, Jun 2001.
- [7] G. Keller, K. Held, V. Eyert, D. Vollhardt, and V. I. Anisimov. Electronic structure of paramagnetic V_2O_3 : Strongly correlated metallic and Mott insulating phase. *Phys. Rev. B*, 70(20):205116, 2004.
- [8] M. S. Laad, L. Craco, and E. Müller-Hartmann. Orbital switching and the first-order insulator-metal transition in paramagnetic V_2O_3 . *Phys. Rev. Lett.*, 91(15):156402, Oct 2003.

* We can thus distinguish different origins of spectral weight. Yet, we cannot tell apart contributions within the \mathcal{L} -block. While one can suppress selected transitions by setting to zero Fermi-velocity matrix elements, contributions are in that case not additive.

- [9] M. S. Laad, L. Craco, and E. Muller-Hartmann. Orbital-selective insulator-metal transition in V_2O_3 under external pressure. *Phys. Rev. B*, 73(4):045109, 2006.
- [10] V. I. Anisimov, D. E. Kondakov, A. V. Kozhevnikov, I. A. Nekrasov, Z. V. Pchelkina, J. W. Allen, S.-K. Mo, H.-D. Kim, P. Metcalf, S. Suga, A. Sekiyama, G. Keller, I. Leonov, X. Ren, and D. Vollhardt. Full orbital calculation scheme for materials with strongly correlated electrons. *Phys. Rev. B*, 71(12):125119, 2005.
- [11] Alexander I. Poteryaev, Jan M. Tomczak, Silke Biermann, Antoine Georges, Alexander I. Lichtenstein, Alexey N. Rubtsov, Tanusri Saha-Dasgupta, and Ole K. Andersen. Enhanced crystal-field splitting and orbital-selective coherence induced by strong correlations in V_2O_3 . *Phys. Rev. B*, 76(8):085127, 2007.
- [12] W. F. Brinkman and T. M. Rice. Application of gutzwiller’s variational method to the metal-insulator transition. *Phys. Rev. B*, 2(10):4302–4304, Nov 1970.
- [13] Jan M. Tomczak and S. Biermann. Effective band structure of correlated materials: the case of VO_2 . *J. Phys.: Cond. Matter*, 19(36):365206, 2007.
- [14] Jan M. Tomczak, F. Aryasetiawan, and S. Biermann. Effective bandstructure in the insulating phase versus strong dynamical correlations in metallic VO_2 . *Phys. Rev. B*, 78(11): 115103, 2008
- [15] F. Rodolakis, B. Mansart, J.P. Rueff, P. Vilmercati, L. Petaccia, A. Goldoni, S. Lupi, P. Metcalf, and M. Marsi. Mott-Hubbard transition in Cr-doped V_2O_3 studied with low energy photoemission. *unpublished, private communication*, 2008.
- [16] A. J. Millis. Optical conductivity and correlated electron physics. In L. Degiorgi D. Baeriswyl, editor, *Strong Interactions in Low Dimensions*, volume 25, page 195ff. Physics and Chemistry of Materials with Low-Dimensional Structures, 2004.
- [17] Anil Khurana. Electrical conductivity in the infinite-dimensional Hubbard model. *Phys. Rev. Lett.*, 64(16):1990, Apr 1990.
- [18] Jan M. Tomczak and S. Biermann. Materials design using correlated oxides: Optical properties of vanadium dioxide. 2008. submitted to *Phys. Rev. Lett*, preprint: arXiv:0807.4044.
- [19] Jan M. Tomczak and S. Biermann. Optical properties of correlated materials - or why intelligent windows may look dirty. Ψ_k *Scientific Highlight of the Month*, no. 88, August 2008. http://www.psi-k.org/newsletters/News_88/Highlight_88.pdf
- [20] M. J. Rozenberg, G. Kotliar, H. Kajueter, G. A. Thomas, D. H. Rapkine, J. M. Honig, and P. Metcalf. Optical conductivity in Mott-Hubbard systems. *Phys. Rev. Lett.*, 75(1):105–108, Jul 1995.
- [21] Per-Olov Löwdin. A note on the quantum-mechanical perturbation theory. *J. Chem. Phys.*, 19(11):1396, Nov 1951.
- [22] O. K. Andersen and T. Saha-Dasgupta. Muffin-tin orbitals of arbitrary order. *Phys. Rev. B*, 62(24):R16219–R16222, Dec 2000.
- [23] M. M. Qazilbash, A. A. Schafgans, K. S. Burch, S. J. Yun, B. G. Chae, B. J. Kim, H. T. Kim, and D. N. Basov. Electrodynamics of the vanadium oxides VO_2 and V_2O_3 . *Phys. Rev. B*, 77(11):115121, 2008.
- [24] L. Baldassarre, A. Perucchi, D. Nicoletti, A. Toschi, G. Sangiovanni, K. Held, M. Capone, M. Ortolani, L. Malavasi, M. Marsi, P. Metcalf, P. Postorino, and S. Lupi. Quasiparticle evolution and pseudogap formation in V_2O_3 : An infrared spectroscopy study. *Phys. Rev. B*, 77(11):113107, 2008.
- [25] E Pavarini, A Yamasaki, J Nuss, and O K Andersen. How chemistry controls electron localization in $3d^1$ perovskites: a Wannier-function study. *New Journal of Physics*, 7:188, 2005.